© 2023. Published by The Company of Biologists Ltd | Development (2023) 150, dev201220. doi:10.1242/dev.201220

RESEARCH ARTICLE

TECHNIQUES AND RESOURCES

In vivo profiling of the Zucchini proximal proteome in the *Drosophila* ovary

Thi Thanh My Nguyen[1,*], Choijamts Munkhzul[1,2,*], Jeesoo Kim[3,4], Yeonju Kyoung[3,4], Michele Vianney[1,2], Sanghee Shin[3,4], Seonmin Ju[3,4], Hoang-Anh Pham-Bui[1,2], Junhyung Kim[1,2], Jong-Seo Kim[3,4,‡] and Mihye Lee[1,2,‡]

ABSTRACT

PIWI-interacting RNAs (piRNAs) are small RNAs that play a conserved role in genome defense. The piRNA processing pathway is dependent on the sequestration of RNA precursors and protein factors in specific subcellular compartments. Therefore, a highly resolved spatial proteomics approach can help identify the local interactions and elucidate the unknown aspects of piRNA biogenesis. Herein, we performed TurboID proximity labeling to investigate the interactome of Zucchini (Zuc), a key factor of piRNA biogenesis in germline cells and somatic follicle cells of the *Drosophila* ovary. Quantitative mass spectrometry analysis of biotinylated proteins defined the Zuc-proximal proteome, including the well-known partners of Zuc. Many of these were enriched in the outer mitochondrial membrane (OMM), where Zuc was specifically localized. The proximal proteome of Zuc showed a distinct set of proteins compared with that of Tom20, a representative OMM protein, indicating that chaperone function-related and endomembrane system/vesicle transport proteins are previously unreported interacting partners of Zuc. The functional relevance of several candidates in piRNA biogenesis was validated by derepression of transposable elements after knockdown. Our results present potential Zuc-interacting proteins, suggesting unrecognized biological processes.

KEY WORDS: *Drosophila*, Proximity labeling, TurboID, Zucchini, PiRNA

INTRODUCTION

PIWI-interacting RNAs (piRNAs) are small RNAs (24-31 nucleotides in length) that play a conserved role in maintaining the genome integrity by silencing transposable elements (Czech et al., 2018; Huang et al., 2017; Iwasaki et al., 2015). It is one of the three major classes of small RNAs that are loaded onto the Argonaute (Ago) family proteins and guide target repression (Hutvagner and Simard, 2008; Ozata et al., 2019). While miRNA and siRNA, the other two classes of small RNAs, and their partner Ago proteins are ubiquitously expressed, piRNAs and PIWI clade Ago proteins are predominantly expressed in animal gonads where they defend the germline genome (Höck and Meister, 2008; Ozata et al., 2019). In addition to their classic role in silencing selfish genetic elements, piRNAs have recently been shown to regulate mRNA expression and it is further suggested that they are implicated in various diseases, including cancer (Liu et al., 2019; Wang and Lin, 2021).

piRNAs are processed from long precursor RNAs that are transcribed from genomic loci harboring transposable element sequences (Watanabe and Lin, 2014). The piRNA precursors are transported from the nucleus to specialized cytoplasmic compartments, such as nuage (germline cells), Yb body (somatic follicle cells) and the mitochondrial outer membrane, in which the piRNA processing machinery is enriched (Ge et al., 2019; Munafò et al., 2019; Qi et al., 2011; Saito et al., 2010; Voronina et al., 2011). Whereas miRNA and siRNA are processed from double-stranded RNA precursors that have signatures of secondary structure and sequence motifs recognized by the specific endonuclease, Dicer, piRNA single-stranded precursors do not share prominent features (Le Thomas et al., 2014). Hence, the underlying mechanism of precursor selection for piRNA processing remains largely unsolved, and proper localization of precursors in the processing centers has been proposed to be crucial for initiating the production of mature piRNAs. The artificial tethering of a reporter RNA to the components of the nuage or Yb body leads to its processing (Pandey et al., 2017; Rogers et al., 2017).

piRNA processing is mediated by two representative pathways: Zucchini (Zuc)-mediated processing and ping-pong processing (Aravin et al., 2007). Zuc is an endonuclease localized on the outer membrane of the mitochondria (Pane et al., 2007; Saito et al., 2010). It mediates the cleavage of precursors to generate the phased pattern of piRNAs, simultaneously defining the 3′-end of an upstream region and 5′-end of a downstream region (Ding and Chen, 2020; Huang et al., 2017; Malone et al., 2009). Reciprocal cleavage by Aub and Ago3 generates mature piRNAs through the ping-pong loop in nuage, which is the perinuclear electron-dense structure (Brennecke et al., 2007; Gunawardane et al., 2007). In the ping-pong pathway, the slicing of the transposon RNA guided by complementary piRNA provides substrates for additional piRNA production, which enables the amplification of piRNAs that target active transposons (Czech and Hannon, 2016; Shpiz et al., 2014). Each piRNA processing pathway is strongly dependent on protein factors enriched in specific subcellular compartments, as was observed in the splicing or rRNA maturation pathways (Huang et al., 2017; Lim and Kai, 2007; Ma et al., 2009; Saito et al., 2010). Therefore, a localization-based approach can help elucidate the unknown aspects of piRNA biogenesis.

The proximity labeling method sheds light on protein interaction networks based on spatially resolved proteome mapping. Existing biochemical methods to investigate protein-protein interactions

[1]Soonchunhyang Institute of Medi-bio Science, Soonchunhyang University, Cheonan 31151, Korea. [2]Department of Integrated Biomedical Science, Soonchunhyang University, Cheonan 31151, Korea. [3]Center for RNA Research, Institute for Basic Science, Seoul 08826, Korea. [4]School of Biological Sciences, Seoul National University, Seoul 08826, Korea.
*These authors contributed equally to this work

‡Authors for correspondence (mihyelee@sch.ac.kr; jongseokim@snu.ac.kr)

T.T.M.N., 0000-0003-0902-6234; C.M., 0000-0002-9239-366X; M.V., 0000-0003-3894-734X; S.S., 0000-0002-8786-6995; H.-A.P.-B., 0000-0001-8444-0609; J.K., 0000-0001-8655-4298; M.L., 0000-0001-9689-6937

Handling Editor: Swathi Arur
Received 23 August 2022; Accepted 24 January 2023

Development (2023) 150, dev201220. doi:10.1242/dev.201220

(PPIs) are advantageous only for studying stable protein interactions that can resist the harsh conditions required for protein complex purification, or valid only under experimentally reconstituted conditions (Mehla et al., 2017; ten Have et al., 2011). Microscopy-based imaging methods have also been used to address PPIs based on colocalization under a wide range of resolutions; however, these methods can simultaneously analyze only a handful of proteins and are impractical as high-throughput large-scale discovery methods. The development of proximity labeling methods enables a systemic approach *in vivo* for PPIs through the spatial mapping of proteins (Choi-Rhee et al., 2004; Qin et al., 2021; Roux et al., 2012). In these methods, the engineered enzyme fused to the target protein generates reactive molecules, most commonly biotin, that covalently and selectively label proximate proteins. The short-lived reactive molecules are quickly quenched, which allows the labeling of proteins within a radius of ∼10-20 nm. Biotinylated proteins were isolated and further identified using mass spectrometry. *In vivo* labeling can detect not only weak and transient interactions, but also physiological associations, while maintaining intact subcellular structures and protein complex integrity (Nguyen et al., 2020). The proximity labeling method BioID uses a promiscuous R118G mutant of BirA, biotin ligase, which requires ATP and biotin to produce the reactive biotin-AMP that acts on the primary amines (e.g. lysine side chains) of proximate proteins (Varnaitė and MacNeill, 2016). APEX, an engineered ascorbate peroxidase, oxidizes biotin-phenol to phenoxyl radicals in the presence of H_2O_2, which reacts with the electron-dense side chains of amino acids (e.g. tyrosine) (Rhee et al., 2013). Both have been widely used for PPI studies; however, each has a different drawback. APEX-based proximity labeling requires H_2O_2, which can be cytotoxic, and the BioID labeling rate is slow compared with the robust enzyme kinetics of APEX (Qin et al., 2021). Recently, TurboID, a modified version of BioID, was developed by screening BirA variants generated from directed evolution, enabling non-toxic proximity labeling within 10 min (Branon et al., 2018). Moreover, TurboID efficiently induced biotinylation in worms and flies, in contrast to BioID, which has low catalytic activity; therefore, TurboID could possibly be applied to a wide range of *in vivo* proximity labeling (Baker et al., 2021; Branon et al., 2018; Uçkun et al., 2021; Zhang et al., 2021).

Here, we attempted proximity labeling in *Drosophila* ovaries to investigate the interactome of Zuc. We induced the biotinylation of proteins in the vicinity of Zuc using TurboID and identified the biotinylated proteins using highly sensitive mass spectrometry. Through quantitative analysis, Zuc-proximal proteins were identified in the germline and follicle cells of the ovary tissue, including well-known interactors of Zuc in piRNA biogenesis. Interestingly, protein folding, membrane organization and vesicle-trafficking-related proteins were found to be previously unreported interactors of Zuc. We also validated the implications of several candidates in the regulation of transposable elements, which suggests their functional relationship with Zuc-mediated piRNA biogenesis. This study showed that proximity labeling could be a valuable tool for the discovery of interacting proteins.

RESULTS

Proximity labeling of a piRNA processing factor, Zuc, in *Drosophila* ovary

Zuc, a key factor in piRNA processing in *Drosophila*, functions as an endonuclease on the outer mitochondrial membrane (OMM) to produce phased piRNAs in somatic ovarian follicle cells and germline cells (Haase et al., 2010; Ipsaro et al., 2012; Nishimasu et al., 2012; Pane et al., 2007). To explore the unknown interaction partners of Zuc in the piRNA processing pathway, we used the TurboID proximity labeling method in *Drosophila* ovaries. Transgenic flies expressing Zuc-V5-TurboID, Nuclear export signal (NES)-V5-TurboID and Tom20-V5-TurboID were generated. An NES that facilitates the protein translocation from the nucleus to the cytoplasm was added to the V5-TurboID for cytoplasmic TurboID control. Tom20, a representative OMM protein, was fused to V5-TurboID to prepare an OMM-localized TurboID control. Each TurboID fusion protein was overexpressed in the ovarian germline cells of *matα*-Gal4/UAS-TurboID female flies. We then induced biotinylation by feeding female adult flies with food containing 100 µM biotin, followed by ovary tissue isolation and subsequent analysis (Fig. 1A).

NES-TurboID, Tom20-TurboID and Zuc-TurboID showed a substantial increase in biotinylated proteins compared with the wild-type control (Fig. 1B). Longer exposure of the flies to biotin enhanced the signal intensities of TurboID-specific biotinylated proteins, as was observed by western blotting using streptavidin-HRP (Fig. 1B; Fig. S1A). Overexpressed TurboID proteins fused to different targets localized in a characteristic pattern in germline cells (Fig. 1C). NES-TurboID proteins were found dispersed in the cytoplasm, and Tom20-TurboID proteins were colocalized with the mitochondrial marker ATP5α. Zuc-TurboID proteins mostly overlapped with the mitochondria, as expected. Biotinylated proteins were specifically detected based on TurboID expression in all three samples (Fig. 1D). TurboID expression in ovarian germline cells did not affect fertility. The hatching rate of eggs laid by TurboID-expressing females (*matα*-Gal4/UAS-TurboID) also did not differ from that of the control (Fig. S1B).

APEX proximity labeling was also attempted, based on previously published studies in *Drosophila* tissue (Fig. S1C) (Chen et al., 2015; Mannix et al., 2019). APEX2 alone induced significant biotinylation, which was clearly detected by western blotting (Fig. S1D). However, Zuc-APEX2 did not show an increase in biotinylated proteins compared with the control, indicating low efficiency of proximal labeling (Fig. S1D).

Identification of Zuc proximal proteome through quantitative proteomics

To screen Zuc-interacting proteins, we conducted proteomic profiling of biotinylated proteins in the Zuc-TurboID ovary tissue samples via liquid chromatography and tandem mass spectrometry (LC-MS/MS) analysis in biological triplicates. Two control samples, NES-TurboID and Tom20-TurboID were included for quantitative proteomics. Endogenously biotinylated proteins in *Drosophila* ovary samples can be controlled by NES-TurboID and Tom20-TurboID. NES-TurboID induces biotinylation of abundant cytoplasmic proteins, which can also control a broad range of non-specific labeling detected in Zuc-TurboID samples. Tom20-TurboID is expected to biotinylate Tom20-specific proximal proteins, but may also induce non-specific labeling of abundant OMM proteins. Therefore, the biotinylated protein profile of Tom20-TurboID is useful to exclude non-specific labeling of the OMM protein in Zuc-TurboID samples and define a distinct protein with Zuc-TurboID specificity beyond OMM localization dependency. We first performed trypsin digestion of NES-, Tom20- or Zuc-TurboID proteomes and efficiently purified biotinylated peptides using streptavidin beads. We then directly identified the biotinylated lysine residue by MS/MS analysis (Lee et al., 2017). Approximately 3000 and 5000 biotin-labeled peptides were non-redundantly identified in the NES-/Zuc-TurboID samples

Development (2023) 150, dev201220. doi:10.1242/dev.201220

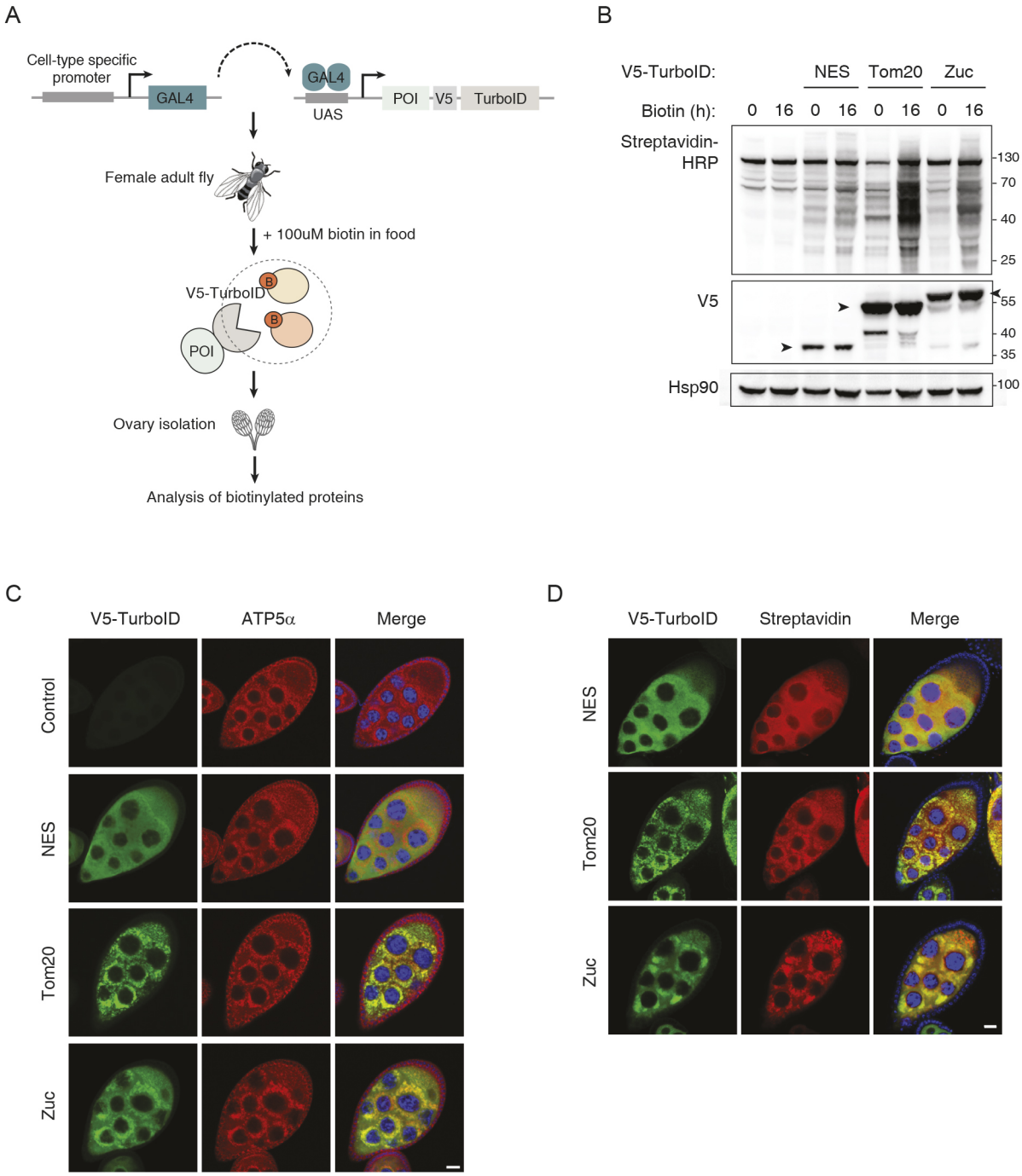

Fig. 1. TurboID-mediated proximity labeling in *Drosophila* ovary. (A) Schematic of TurboID proximity labeling in *Drosophila* tissue. POI, protein of interest. TurboID fusion proteins are expressed in a specific cell population using UAS/GAL4 system. The biotinylation of TurboID-proximate proteins is strongly induced *in vivo* by supplementing biotin in fly food. Whole ovaries were dissected from female flies for further analysis. (B-D) The *matα*-Gal4/UAS-TurboID ovary samples were used for the analysis. (B) TurboID expressions and biotinylated proteins in western blotting. NES-, Tom20- and Zuc-V5-TurboID proteins in ovary tissue samples were detected with anti-V5 antibody at the expected size. The fused proteins are indicated by the arrowheads. TurboID-expressing ovary samples show higher levels of biotinylated proteins compared with the control sample; when fed with biotin-supplemented food for 16 h, biotinylated protein levels are substantially higher. (C) Localization of TurboID fusion proteins in the germline cells of ovary tissue. Immunofluorescence images show the localization of TurboID fusion proteins (V5, green) with the pattern of mitochondria (ATP5α, red). The control is *matα*-Gal4/+ without TurboID expression. (D) Fluorescence imaging of TurboID labeling in germline cells. The distributions of biotinylated proteins (Streptavidin, red) largely overlap with the TurboID fusion protein expressions (V5, green). DAPI was used as a nuclear counterstain (blue). Scale bars: 20 µm.

and the Tom20-TurboID sample, respectively (Fig. S2A). We generated a biotinylated protein list with quantitative intensity by integrating the corresponding intensities of biotinylated peptides for NES-, Tom20- and Zuc-TurboID samples (Fig. 2A). Notably, our quantitative proteomics data for biotin-labeled proteins were highly reproducible between replicates (Fig. S2B). Principal component analysis identified distinct sets of proteins in the NES-, Tom20- and Zuc-TurboID samples (Fig. 2B). Collectively, we identified 1382

Development (2023) 150, dev201220. doi:10.1242/dev.201220

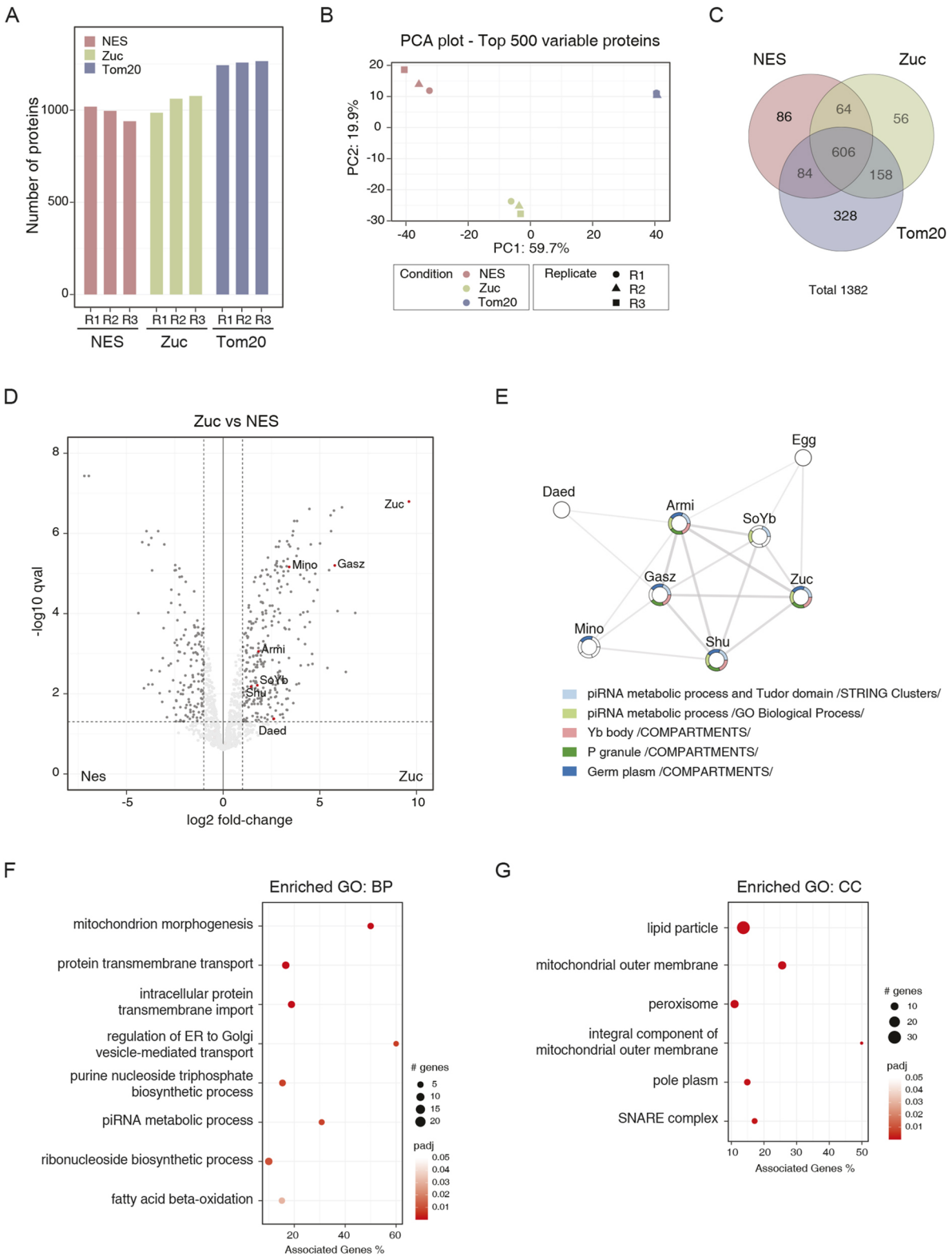

Fig. 2. Proteomic analysis of Zuc-TurboID proximity labeling. (A) The number of biotinylated proteins detected in each replicate of NES-, Tom20- and Zuc-TurboID samples. (B) Principal component analysis (PCA) plot of top 500 proteins in each replicate of NES-, Tom20- and Zuc-TurboID samples. (C) Venn diagram of biotinylated protein lists in NES-, Tom20- and Zuc-TurboID samples. The lists include commonly detected proteins in triplicates of each TurboID sample. (D) Volcano plot of NES- and Zuc-TurboID. Several piRNA pathway-related proteins are marked in the plot. Differential expression analysis was performed by protein-wise linear models combined with empirical Bayes statistics. (E) Interconnected nodes containing Zuc, based on the analysis of Zuc proximal proteins using STRING database (Zuc proximal proteins: fold change >2, q-value<0.05, compared with NES-TurboID). (F,G) GO enrichment of Zuc proximal proteins. The dot plot depicts the significantly overrepresented biological processes and cellular component pathways (*P*.adj<0.05). (F) GO biological process enrichment. (G) GO cellular compartment enrichment. The significance (F,G) was calculated with a two-sided hypergeometric test and Bonferroni step-down method was used for *P*-value adjustment.

Development (2023) 150, dev201220. doi:10.1242/dev.201220

proteins from all NES-, Tom20- and Zuc-TurboID samples, in which we counted the proteins which were reproducibly detected in triplicate experiments for the respective samples (Fig. 2C; Fig. S2C; Table S1). Note that 1382 proteins were used in all subsequent pairwise statistical comparison after the missing quantity value for the respective protein at any replicate was substituted with the statistically imputed value.

To define the proximal proteome of Zuc, biotinylated proteins significantly enriched in Zuc-TurboID were analyzed in comparison with NES-TurboID. We determined 275 proteins as proximal proteins of Zuc (fold change>2, q-value<0.05) (Fig. 2D; Table S2). We analyzed the known PPIs for these proteins using the STRING database, which revealed several PPI clusters. One of the clusters showed interconnected associations with piRNA-related proteins, including Armi, Gasz, Mino, Shu, SoYb, Daed, Egg and Zuc (Fig. 2D,E). Next, we analyzed gene ontology (GO) enrichment. As expected, piRNA metabolic processes appeared to be enriched in the gene list of the Zuc proximal proteome. This result suggests that TurboID-mediated proximity labeling can provide a reliable interactome of Zuc. In line with the subcellular localization of Zuc on the OMM, enriched GO terms of biological processes are linked to mitochondrion morphogenesis and metabolism-related processes (Fig. 2F). In addition, protein transport-related processes such as endoplasmic reticulum (ER)-to-Golgi vesicle-mediated transport and protein transmembrane transport were found. In the cellular compartment, proximal proteins of Zuc were enriched in lipid particles, mitochondrial outer membranes, peroxisomes and SNARE complexes that pull the membranes in close proximity and mediate vesicle fusion, which is consistent with the results obtained from GO enrichment of biological processes (Fig. 2G).

By applying the identical quantitative criteria (fold change>2 and q-value<0.05), we found 529 proteins proximal to Tom20, which included well-known proteins localized to the OMM, such as Tom40, Mul1, Marf, Spoon, Porin and Tom70 (Fig. 3A,B; Table S2). The strong activity of Tom20-TurboID observed using western blotting (Fig. 1B) may allow the detection of a large number of biotinylated proteins with a higher intensity compared with NES-TurboID. Although false-positive hits from nonspecific biotinylation cannot be excluded, we expect that this analysis may expand the Tom20 interactome, including transiently localized proteins or low-abundance proteins in the vicinity of Tom20. GO enrichment analysis of the biological processes showed that Tom20 proximal proteins are primarily involved in mitochondria-related biological processes, such as mitochondrion organization/morphogenesis/translation, aerobic respiration and metabolic processes (Fig. 3C). The mitochondrial membrane or intracellular organelles were found to be enriched in GO terms of the cellular compartment, indicating that biotin labeling was efficiently induced in the proximal region of Tom20 on the OMM (Fig. 3D). Zuc and Tom20 were both localized on the OMM, but the enriched GO terms for their proximal proteins were different. This result indicates that the proximal proteomes in this analysis have target protein specificity beyond subcellular localization dependency.

Characterization of Zuc-specific proximal proteome

To identify the unique subset of proteins in the Zuc and Tom20 proximal proteomes, we categorized the biotinylated proteins into four clusters depending on the differential intensity patterns in the NES-, Tom20- and Zuc-TurboID samples. To exclude endogenous or nonspecific biotinylated proteins, we used 1140 proteins with q-value <0.05 in any combination of comparisons (NES versus Tom20, NES versus Zuc or Tom20 versus Zuc) (Fig. 4A; Table S3). The specifically enriched proteins in the Zuc-TurboID comprise cluster 2. GO analysis of cluster 2 proteins revealed strong enrichment of the biological process in endomembrane system organization, chaperone-mediated protein folding and regulation of vesicle-mediated transport from ER to Golgi (Fig. 4B). The enriched GO terms of the cellular component included cytoplasmic ribonucleoprotein granules, peptidase complexes and SNARE complexes (Fig. 4C). Several heat shock protein and chaperone-related proteins such as Hsp90, Shu and Hop (also known as Stip1) have been reported to be involved in piRNA biogenesis (Izumi et al., 2013; Karam et al., 2017; Olivieri et al., 2012; Preall et al., 2012; Specchia et al., 2010; Xiol et al., 2012). Additional heat shock and chaperone proteins were found in the Zuc proximal proteome of this study, suggesting that they are the unknown components of the protein folding functional complex for piRNA biogenesis. Zuc is the *Drosophila* homolog of MitoPLD, a member of the phospholipase D superfamily, which generates the signaling lipid phosphatidic acid (PA) from the predominant membrane phospholipid, phosphatidylcholine (Cazzolli et al., 2006; Choi et al., 2006; Huang et al., 2011; Watanabe et al., 2011). PA acts as a membrane anchor to recruit SNARE complex proteins and activate the vesicle trafficking machinery (Starr et al., 2019; Vicogne et al., 2006; Zhukovsky et al., 2019). Conversion of PA to diacylglycerol (DAG) is required to form Coat protein complex I (COPI) vesicles that transport the proteins and lipids from the Golgi to the ER (Fernández-Ulibarri et al., 2007; Yang et al., 2008). In line with the function of MitoPLD in the membrane lipid metabolism, GO enrichment of Zuc-specific proximal proteins suggested a previously unreported function of Zuc in the endomembrane system organization and regulation of vesicle-mediated transport.

Cluster 1 was composed of cytoplasmic proteins, biotinylations of which were prominently detected in NES-TurboID (Fig. 4A; Fig. S3; Table S3). Proteins in cluster 1 are associated with gene expression and cellular component organization or biogenesis, covering a broad range of biological functions. Cluster 3 proteins showed stronger biotinylation intensity in Tom20-TurboID than in NES-TurboID (Fig. 4A; Table S3). They were significantly enriched in the biological processes of mitochondrion organization, mitochondrial transport and diverse metabolic processes (Fig. S3). This cluster may be composed of authentic OMM proteins that can be considered as proximal Tom20 proteins. Several Zuc-interacting components of piRNA biogenesis, including Mino and Gasz, which are well known to be localized on the outer membrane of mitochondria, were found in this cluster (Table S3) (Handler et al., 2013; Vagin et al., 2013; Yamashiro et al., 2020). The biotinylation intensities of cluster 4 proteins were relatively higher in Tom20-TurboID than in NES-TurboID and Zuc-TurboID (Fig. 4A; Table S3). These proteins showed expansive GO enrichment for organelle organization, cellular metabolism and cellular localization (Fig. S3).

Zuc proximal proteins defined commonly in ovarian germline cells and follicle cells

The Zuc-dependent piRNA processing pathway is active in ovarian somatic follicle cells and germline cells. We carried out TurboID-mediated proximity labeling of Zuc in the follicle cells. We isolated ovary tissues that expressed Zuc-TurboID under the control of *tj*-Gal4, specifically in follicle cells, and analyzed them in the same way as was previously described. Follicle cell-specific expression of TurboID was confirmed using immunostaining (Fig. 5A). Western blotting revealed TurboID-mediated biotinylation of proteins,

Development (2023) 150, dev201220. doi:10.1242/dev.201220

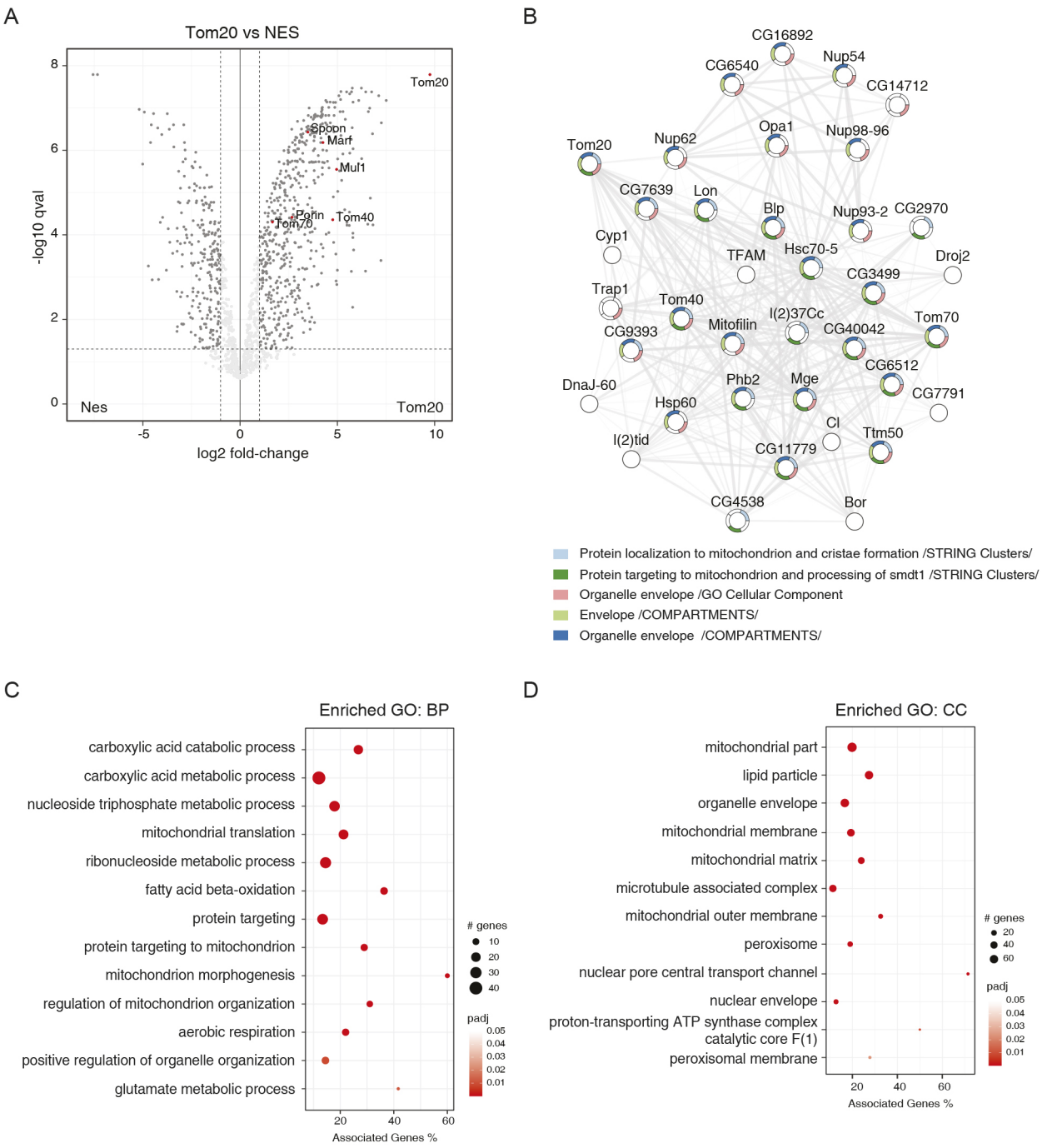

Fig. 3. Proteomic analysis of Tom20-TurboID proximity labeling. (A) Volcano plot of NES- and Tom20-TurboID. Well-known outer mitochondrial membrane proteins are marked in the plot. Differential expression analysis was performed by protein-wise linear models combined with empirical Bayes statistics. (B) Interconnected nodes containing Tom20 based on the analysis of Tom20 proximal proteins using STRING database (Tom20 proximal proteins: fold change >2, q-value<0.05, compared with NES-TurboID). (C,D) GO enrichment of Tom20 proximal proteins. The significance was calculated with a two-sided hypergeometric test and Bonferroni step-down method was used for *P*-value adjustment. The dot plot depicts the significantly overrepresented biological processes (C) and cellular component (D) pathways (*P*.adj<0.05).

which was enhanced by biotin supplementation (Fig. 5B). However, biotinylated proteins appeared at lower levels in follicle cells than in ovarian germline cells. The low efficiency of proximity labeling in follicle cells reduced the enrichment of biotinylated peptides and the identification of proteins in subsequent proteomic analysis. From the proteome data, we analyzed 273 biotinylated proteins, only including proteins detected in triplicate for each condition (Table S1). Statistical analysis identified 137 Zuc-proximal proteins, including Gasz and Armi (Fig. 5C; Table S2). Mino and Shu, well-known factors of the piRNA biogenesis pathway in both germline and follicle cells, were not detected in the Zuc proximal proteome of follicle cells, probably because of the low efficiency of proximity labeling in follicle cells. However, Fs(1)Yb, a soma lineage Yb body component, was specifically found as a Zuc proximal protein in follicle cells, indicating the sensitivity of TurboID-mediated proximity labeling (Fig. 5C,D). In the Zuc

Development (2023) 150, dev201220. doi:10.1242/dev.201220

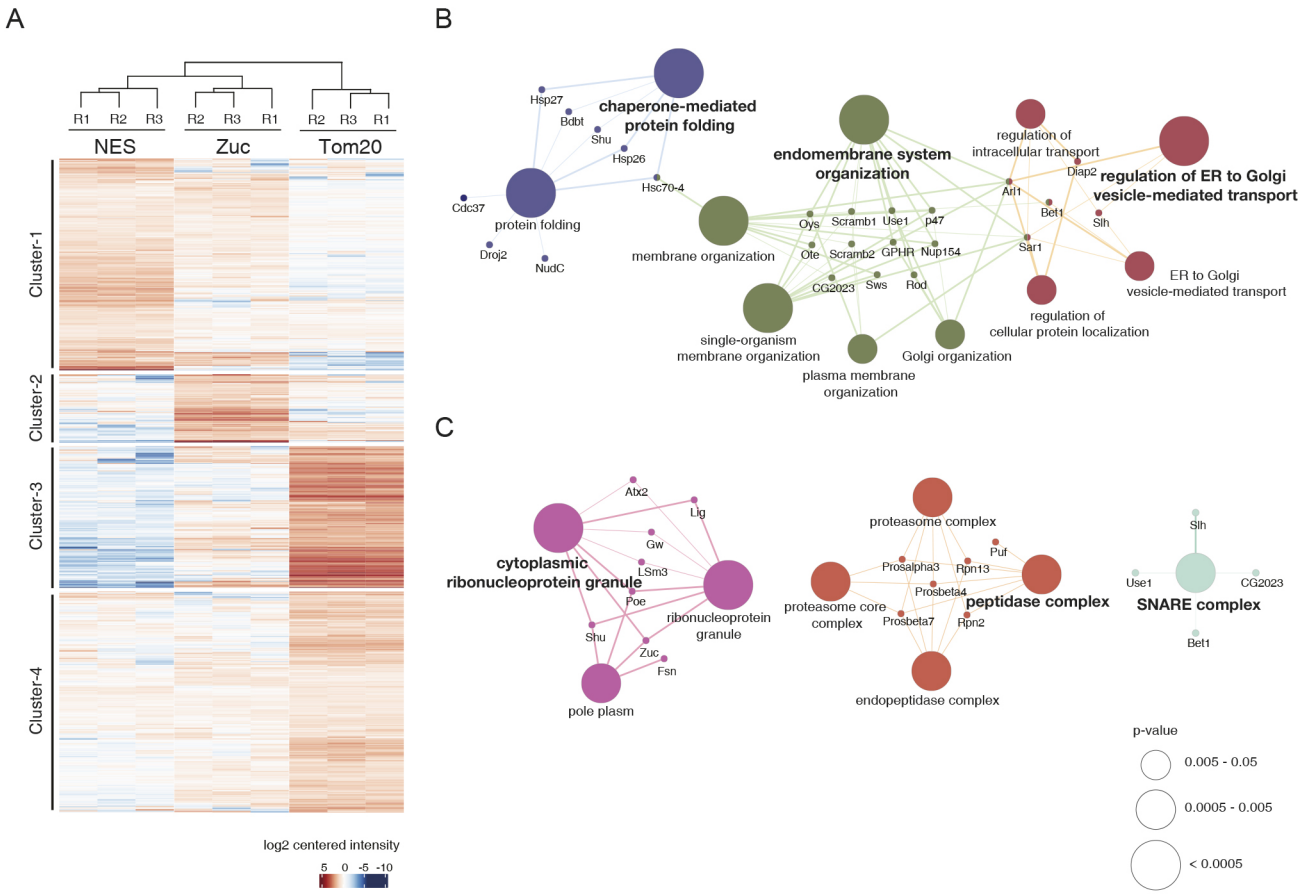

Fig. 4. Zuc-TurboID specific proximity labeling. (A) Classification of proteins according to differential intensity of biotinylation in NES-, Tom20- and Zuc-TurboID samples. Four clusters are shown in the heatmap. (B,C) ClueGO enrichment of cluster 2 proteins. Each node represents pathway GO terms, and node size indicates the level of significance. (B) ClueGO biological process enrichment. (C) ClueGO cellular compartment enrichment. The significance was calculated with two-sided hypergeometric test.

proximal proteome of follicle cells, we also detected a Zuc-containing cluster of PPIs using the STRING database, in which Zuc is linked to piRNA metabolic process-related proteins and membrane/vesicle trafficking or protein folding-related proteins (Fig. 5D). The Zuc proximal proteins in follicle cells showed a large overlap with those in the germline cells (Fig. 5F; Table S2). They also showed the GO enrichment of biological processes in membrane organization and protein folding (Fig. 5E), which is similar to the GO analysis results of Zuc-specific proximal proteins in germline cells. Taken together, these results provide reliable candidates for the Zuc-interacting proteins confirmed in two different cell types, indicating that the Zuc interaction network is preserved in both germline and follicle cells. On the other hand, our proteomic data also showed distinct groups of Zuc-proximal proteins in germline or follicle cells, which suggests cell-type specific features of Zuc-dependent piRNA biogenesis pathway.

The novel candidates of Zuc interacting proteins are involved in the silencing of transposable elements

The proximal proteome of Zuc provides candidates for Zuc-interacting proteins that must be further validated. Interestingly, we found several candidates that have already been identified as Zuc-associated proteins from immunoprecipitation-based screening (Table S4) (Ge et al., 2019). Among 33 proteins not known to function in piRNA biogenesis that co-immunoprecipitated with Zuc, 17 Zuc proximal proteins including Miga, Spoon, Abcd1 and Exd2 overlapped. We next examined several candidates for their functional relevance in Zuc-mediated piRNA biogenesis. We selected candidate genes in different categories of biological functions and tested whether their knockdown derepressed transposon expression levels (Fig. 6). For 12 selected genes that were significantly depleted in the ovary tissues of *nos*-Gal4/UAS-RNAi flies, we measured the expression levels of germline-dominant transposons such as *HeT-A*, *Jockey*, *Beagle* and *Burdock* (Fig. 6; Fig. S4) (Olivieri et al., 2012; Sokolova et al., 2011; Story et al., 2019). In the protein-folding/chaperon-related group, the knockdown of Hsp27 noticeably altered the expression levels of *HeT-A* and *Burdock* transposons by more than 6-fold compared with the control. Cdc37 knockdown results in a small increase of *HeT-A* level and around an 8-fold increase of *Burdock* level. Upon knockdown of nudC, which is predicted to have unfolded protein-binding activity, the levels of *Jockey*, *Beagle* and *Burdock* were modestly changed. A set of Hsc70/Hsp90 chaperone machinery proteins, Droj2, Hsc70-4 and Hop were previously reported to cause transposon derepression up to ∼16-fold when they were knocked down in germline cells (Cappucci et al., 2019). The vesicle trafficking-related gene, *Slh*, and the membrane organization-associated genes, *oys* and *sws*, also affected the transposon expression levels. The depletions of Zw and Usp14, two candidates with other functions, also resulted in a significant derepression of the *HeT-A* and *Burdock* transposons, at a maximum of 39-fold. In addition, among Zuc proximal proteins, Hsc70-5,

Development (2023) 150, dev201220. doi:10.1242/dev.201220

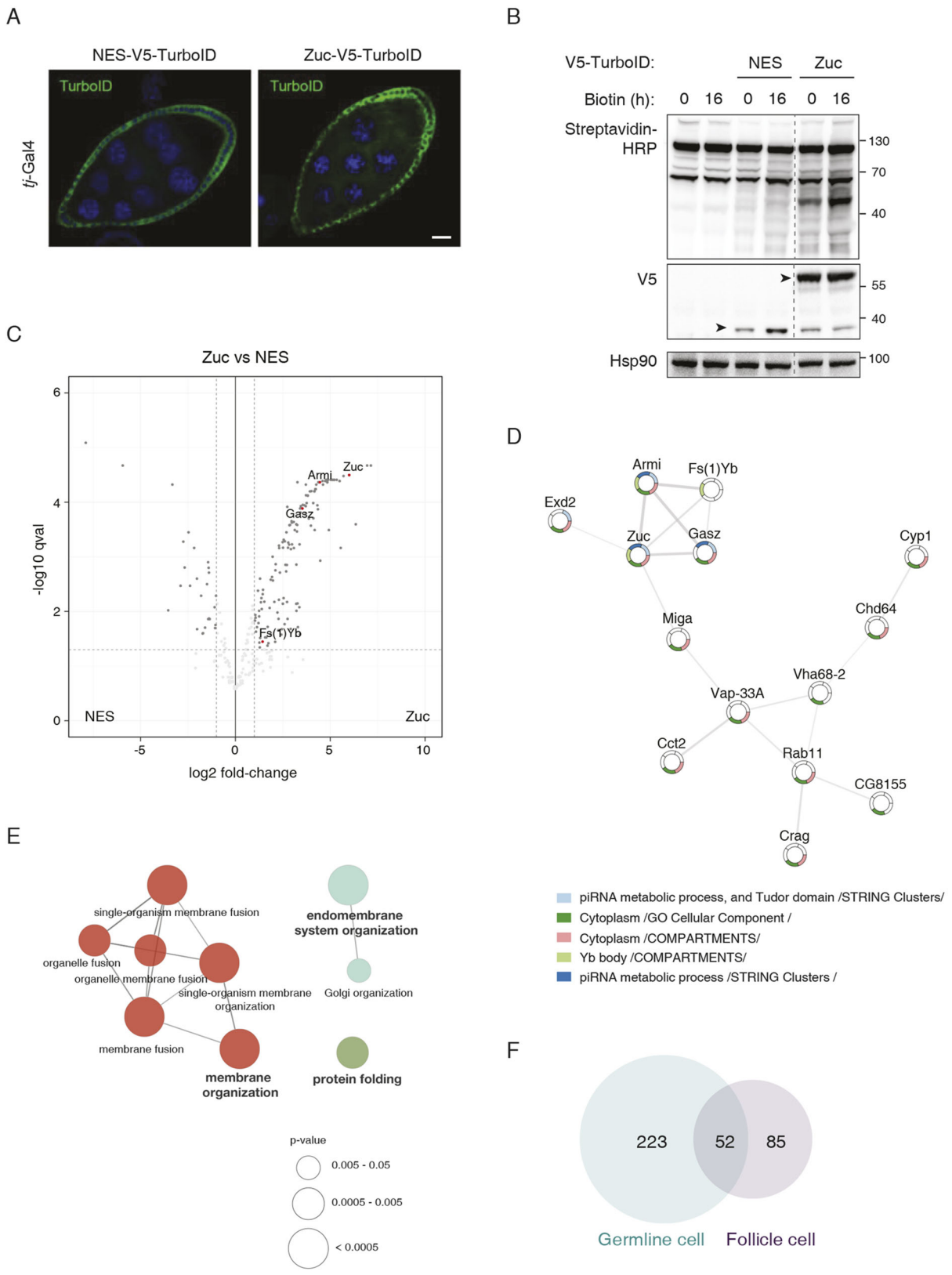

Fig. 5. Zuc-TurboID proximity labeling in follicle cells. (A) V5-TurboID expression in follicle cells of ovary tissue. NES- or Zuc-TurboID expressions induced by *tj*-Gal4 are specifically detected in follicle cells. (B) TurboID expressions and biotinylated proteins in western blotting. NES- and Zuc-V5-TurboID proteins in ovary tissue samples are detected with the anti-V5 antibody (arrowheads). Biotinylated proteins are shown with streptavidin-HRP. (C) Volcano plot of biotinylated proteins in follicle cell samples of NES- and Zuc-TurboID. (D) Interconnected nodes containing Zuc based on the analysis of Zuc proximal proteins using STRING database. (Zuc proximal proteins: fold change >2, q-value<0.05, compared with NES-TurboID). (E) ClueGO biological process enrichment in Zuc proximal proteins. The significance was calculated with a two-sided hypergeometric test. (F) Venn diagram of germline cell- and follicle cell-specific Zuc proximal proteins.

Development (2023) 150, dev201220. doi:10.1242/dev.201220

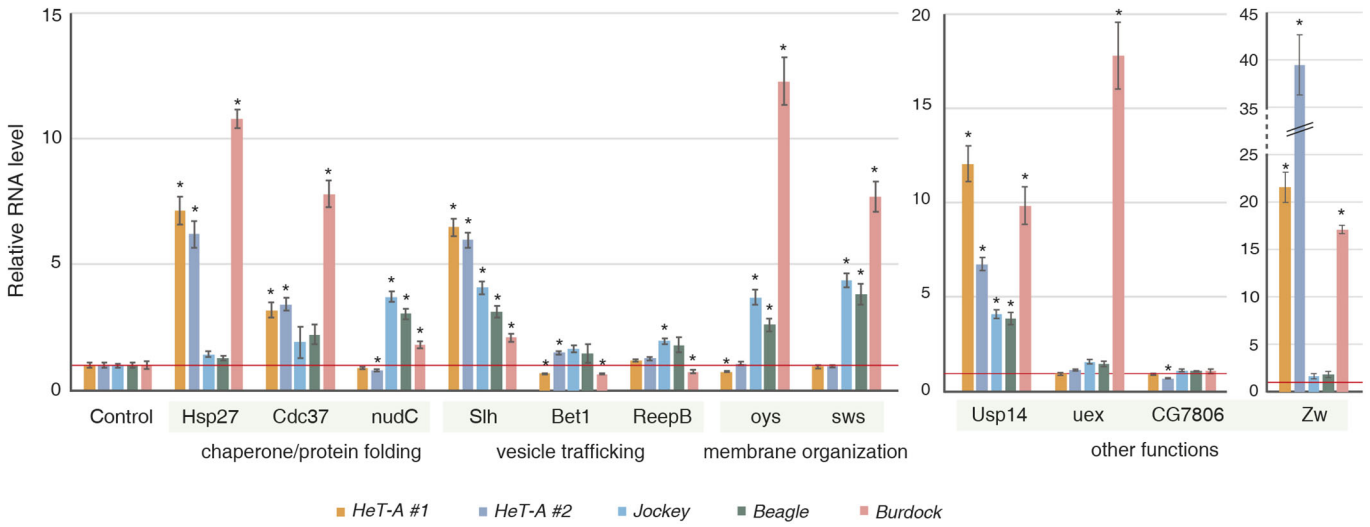

Fig. 6. Zuc interacting candidates are involved in transposon repression. Selected candidates for validation are grouped into biological functions (referring to Fig. 4B). Relative transposon RNA levels were measured in the triplicates of ovary tissue samples (*nos*-Gal4/UAS-RNAi) using quantitative PCR. Four germline dominant transposons were tested after knockdowns of the 12 candidate genes in germline cells. Two different primer sets were used for the *HeT-A* transposon. The RNA levels are normalized to *rp49* and are relative to control (*nos-Gal4*/+) (indicated by red line). Data are presented as mean ±s.e.m. Statistical significance was determined using an unpaired two-tailed Student's *t*-test. **P*<0.05.

Nurf-38, bor, eIF2α and eIF3-S10 (also known as eIF3a) were previously identified as strong candidates required for transposon silencing from RNAi screening (Czech et al., 2013). These results suggest that several Zuc proximal proteins are involved in the repression of transposons, though their knockdown exhibited a small effect compared with Zuc or Armi knockdown (Fig. S4). They may act as an accessory protein or indirectly participate in piRNA biogenesis; the mechanism of their integration into the Zuc-mediated piRNA processing pathway should be further examined.

DISCUSSION

Proximity labeling has opened new avenues to elucidate protein-protein associations through a localization-based approach. The development of diverse enzymes facilitates the application of proximity labeling techniques in a versatile biological context. However, proximity labeling requires optimal expression and catalytic activity of the enzyme, in addition to proper control of the labeling window. Thus, it has not been widely used to study protein interactions *in vivo* using diverse types of animal tissues.

In this study, we investigated the Zuc interactome through the proximity labeling of *Drosophila* ovaries. First, we attempted proximal protein biotinylation using APEX2 *ex vivo*. APEX2 itself showed significant signals of biotinylated proteins in western blotting when the reaction was induced by adding H_2O_2 for 1 min in APEX2-expressing ovary tissue that was previously incubated with biotin-phenol. However, the Zuc-APEX2 fusion protein was expressed at a lower level than APEX2 alone and did not produce biotinylated protein signals above the detection level (Fig. S1D). We applied the TurboID-mediated proximal biotinylation method *in vivo*. Proximal labeling was accomplished by feeding the flies with biotin-supplemented diets; these flies were expressing several target proteins fused to TurboID in the ovary. Although APEX2 is suitable for capturing snapshots of PPIs within 1 min, TurboID improves the biotinylation of proximal proteins by tuning the reaction time, facilitating the optimization of proximity labeling in animal tissues. Together with our results, a growing body of proximity-labeling-related research has emphasized the importance of selecting proximity-labeling enzymes depending on their unique advantages and disadvantages.

The proteomic data of TurboID proximity labeling presented candidates for Zuc-interacting proteins, and these data are statistically significant. Proximity labeling data without quantitative analysis could be candidate lists containing considerable false positives. To minimize false positives, we used proper controls and specified the proximal proteins through the statistical analysis of ovarian germline cells (Han et al., 2018; Hung et al., 2017). However, in the case of ovarian follicle cells, NES-TurboID, which was used as the control for endogenous biotinylated proteins and non-specifically biotinylated abundant proteins, showed low labeling efficiency. The follicle cell sample of NES-TurboID identified a significantly smaller number of biotinylated proteins with lower signal intensity in mass spectrometry than that observed for Zuc-TurboID, which hindered the efficient identification of Zuc-interacting protein candidates through quantitative analysis. Our experience suggests that appropriate control data are crucial for defining a reliable proximal proteome.

Several piRNA biogenesis-related proteins were found in the Zuc proximal proteome of germline cells. These proteins include Shu, Mino, Gasz, Daed and SoYb, which form a STRING network cluster together with Zuc and Armi, indicating that known PPI networks were preserved in our data. However, proteins implicated in the piRNA ping-pong pathway, such as Spn-E and Qin, were not enriched in the Zuc-proximal proteome (Czech et al., 2013; Malone et al., 2009; Zhang et al., 2011). The well-known Zuc-interacting protein Piwi was also not included in the proximal proteome of Zuc. Given the substantial biotinylation levels of these proteins in the NES-TurboID proximal proteome, a large proportion of Piwi, Aub and Ago3 proteins may be more diffused in the cytoplasm, where they are biotinylated. When controlling the background level, proteins with less local enrichment are expected to have disadvantages in quantitative analysis.

The proximal proteins of Zuc include proteins with unknown functions in piRNA biogenesis, a number of which were reported to be physically associated with Zuc using co-immunoprecipitation (Ge et al., 2019; Zhang et al., 2016). In a previous study, Exd2 (exonuclease 3′-5′ domain containing 2), a Zuc proximal protein in germline and follicle cells, was co-immunoprecipitated with Zuc (Ge et al., 2019). These findings suggest that Exd2, like another

Development (2023) 150, dev201220. doi:10.1242/dev.201220

exonuclease Nbr (a fly ortholog of EXD3), may play a role in piRNA processing, (Feltzin et al., 2015; Hayashi et al., 2016). Considering the localization of Exd2 on the OMM, it is necessary to examine whether Exd2 is involved in piRNA processing on the OMM (Hensen et al., 2018; Park et al., 2019). In the Zuc proximal proteome, we also found a group of heat shock proteins and chaperone proteins, among which Shu, Hsp90 and Hop have been previously reported to be involved in piRNA biogenesis (Table S2). This finding suggests that the protein folding-related proteins may form a complex and act with Zuc in the piRNA biogenesis pathway. Interestingly, proteins of endomembrane organization and vesicle trafficking were also presented as candidates for Zuc-interacting proteins, which may be linked to the membrane lipid metabolism mediated by Zuc/MitoPLD. This aspect has not received much attention compared with the endonuclease function of Zuc/MitoPLD. Our data provide clues to understand the additional role of Zuc and address the novel molecular mechanism of piRNA biogenesis in the future. In addition, in this study, we examined the functional involvement of Zuc proximal proteins in piRNA biogenesis indirectly by measuring transposon element levels after the knockdown of several candidates. Although the effect was limited, significant changes in transposon levels upon knockdown were observed, which suggests further investigation is needed to confirm Zuc interacting partners and to elucidate their specific functions in piRNA biogenesis for future research.

Screening through proximity labeling reveals any chance of association, which expands the PPI network. Therefore, the proximal proteome can reveal potential interacting partners and provide further insight into the physiological functions and regulatory mechanisms of the target protein. Given the depth and integrity of our proteomic analysis, screening to identify interacting proteins of Zuc in the *Drosophila* tissue would be excellent to provide reliable and valuable resources by successfully controlling *in vivo* proximity labeling. In the future, integrated analysis of proximal proteomic data and other types of protein interaction studies can generate a comprehensive understanding of PPIs.

MATERIALS AND METHODS

DNA constructs

APEX2 and TurboID fragments were obtained from plasmids pcDNA5 APEX2-V5-YKT6 and pCDNA5 MCP-TurboID-V5 (gifted by Dr Hyun-Woo Rhee, Seoul National University, Korea) by PCR using PrimeSTAR HS DNA Polymerase (Takara). Zuc and Tom20 open reading fragments were amplified from *Drosophila* ovary cDNA generated by reverse transcription using SuperScript III Reverse Transcriptase (Invitrogen). The NES fragment (aa sequence: LALKLAGLDI) was synthesized by referring to the UAS-NES-APEX-Flag plasmid information from a previous study (Chen et al., 2015). For generating transgenic flies, APEX2-V5 or V5-TurboID, together with NES, Zuc or Tom20 fragments, were inserted into the pUASp vector using a homologous recombination method with an In-Fusion HD cloning kit (Takara).

Fly genetics/transgenic flies

Transgenic flies were generated at BestGene Inc. or the Korea *Drosophila* Resource Center (KDRC). Fly lines w^{1118} (BDSC #5905), *mat*α-Gal4 (BDSC #7062) and *nos-VP16*-Gal4 (BDSC #4937) were obtained from the Bloomington *Drosophila* Stock Center, and *tj*-Gal4 (DGRC #104055) was obtained from the Kyoto Stock Center. RNAi lines presented in Table S5 were obtained from the Bloomington *Drosophila* Stock Center. The flies were raised on standard fly food at 25°C.

Proximity labeling in fly tissues

UAS-APEX2 or UAS-TurboID transgenes (APEX2-V5, APEX-V5-Zuc, NES-V5-TurboID, Zuc-V5-TurboID and Tom20-V5-TurboID) were expressed in germline cells using *mat*α-Gal4 and in follicle cells using *tj*-Gal4. For APEX proximity labeling, ovaries were dissected from 4-day-old female flies in Grace's insect medium (Gibco). Isolated ovary tissues were incubated with 500 µM Biotin-phenol (BP) in 1× PBS for 30 min. Next, 30% H_2O_2 was added to a final concentration of 1 mM H_2O_2 to activate APEX labeling for 1 min at 25°C. The reaction was quenched by washing three times with 1× PBS containing 5 mM Trolox, 10 mM sodium azide and 10 mM sodium ascorbate. For TurboID proximity labeling, female flies were grown either on standard food or 100 µM biotin-containing food for 4, 8 or 16 h before isolating the ovary tissues.

Quantitative RT-PCR

Total RNA was prepared from fly ovaries by TRIzol reagent and subsequently treated with DNase I. cDNA was synthesized with 0.5 µg of total RNA through the reverse transcription using PrimeScript RT-PCR kit (Takara) or ReverTra Ace qPCR RT Master Mix (Toyobo). The levels of target RNA were measured by quantitative PCR using SYBR Green PCR Master Mix (Applied Biosystems) or SYBR Green Realtime PCR Master Mix (Toyobo) and normalized to the level of *rp49* (*RpL32*). The primers used for PCR are presented in Table S4.

Western blotting

Fly ovary tissues were homogenized in RIPA lysis buffer [50 mM Tris (pH 8), 150 mM NaCl, 0.1% SDS, 0.5% sodium deoxycholate, 1% Triton X-100, 1× protease inhibitor cocktail (Sigma-Aldrich) and 1 mM PMSF (Thermo Fisher Scientific)] on ice. The lysate supernatant was obtained by centrifugation at 12,000 rpm (13,500 ***g***) for 10 min at 4°C. Proteins were separated on SDS-PAGE gels and transferred to nitrocellulose membranes (GE Healthcare). The membrane was blocked in 2% (w/v) bovine serum albumin in 1× PBST (phosphate-buffered saline, 0.1% Tween 20) for 1 h at room temperature (RT) or overnight at 4°C. Next, the membrane was incubated with primary antibodies overnight at 4°C and subsequently with secondary antibodies for 40 min at RT. For biotinylated protein detection, the membrane was incubated with 0.3 µg/ml streptavidin-HRP in PBST for 1 h at 4°C. Protein bands were detected using Clarity Western ECL Blotting Substrates (Bio-Rad) on a ChemiDoc Imaging System. Primary antibodies used for western blotting in this study were: rabbit α-HSP90 (Cell Signaling Technology, 4874, 1:1000), α-Streptavidin-HRP (Thermo Fisher Scientific, 21126, 0.3 µg/ml), mouse α-V5 (Invitrogen, R96025, 1:1000). Secondary antibodies used for western blotting were: goat anti-rabbit IgG, HRP (Thermo Fisher Scientific, 31460, 1:4000), goat anti-mouse IgG, HRP (Thermo Fisher Scientific, 31430, 1:4000).

Immunofluorescence

Ovary tissues dissected in Grace's insect medium (Gibco) were fixed with 5% (w/v) formaldehyde (Polysciences) in PBS for 30 min at RT. After several washes, the fixed ovaries were incubated with 5% fetal bovine serum (Corning, 35-015-CV) in 1× PBT (phosphate-buffered saline, 0.1% Triton X-100) for 1 h at RT for efficient permeabilization. Next, the ovaries were incubated with anti-V5 (Cell Signaling Technology, 13202, 1:200) and anti-ATP5α (Abcam, ab14748, 1:200) antibodies overnight at 4°C and subsequently incubated with secondary antibodies, Alexa Fluor Plus 488 anti-rabbit IgG (Thermo Fisher Scientific, A32731, 1:200) and Alexa Fluor Plus 594 anti-mouse IgG (Thermo Fisher Scientific, A32742, 1:200). To visualize biotinylated proteins, an Alexa Fluor 594 streptavidin conjugate (Molecular Probes, S11227, 1:300) was used for immunostaining. DAPI (Thermo Fisher Scientific, 62248, 1:1000) in PBS was used as a nuclear counterstain for 5 min at RT before imaging by confocal microscopy.

Embryo hatching rate analysis

Newly eclosed female and male flies were incubated at 25°C for 2-3 days. For embryo collection, flies were placed on fresh grape juice agar plates and allowed to lay eggs for 2 h. The plate was incubated at 25°C for 1 day and the hatching rate was determined by counting the number of larvae hatched from the collected embryos.

Sample preparation for proteomics

Ovary tissues were lysed with lysis buffer [2% SDS in 1× Tris-buffered saline (TBS), 1× protease inhibitor cocktail] and sonicated (Covaris

Development (2023) 150, dev201220. doi:10.1242/dev.201220

M220 ultrasonicator). Cold acetone was added to the lysate for protein precipitation overnight at −20°C. The pellet was then washed with 90% cold acetone and 10% TBS. After air-drying, the pellet was solubilized with 8 M urea in 50 mM ammonium bicarbonate (ABC). A total of 3 mg of protein in 500 µl of 8 M urea, and 50 mM ABC were used for subsequent trypsin digestion. Proteins were denatured for 1 h at 37°C with shaking at 450 rpm and reduced with 10 mM DTT for 1 h at 37°C with shaking at 450 rpm. Proteins were alkylated with 40 mM iodoacetamide at 37°C for 1 h with shaking at 450 rpm. The samples were diluted eight times with 50 mM ABC. $CaCl_2$ was then added at a final concentration of 1 mM. The protein samples were digested with trypsin (Thermo Fisher Scientific, 20233) for 16 h at 37°C at a 1:50 (w/w) trypsin-to-protein ratio. Streptavidin (SA) beads (Invitrogen, 65001) were then added to the samples after several washes with 2 M urea in 1× TBS and incubated for 1 h at RT. The beads were washed twice with 2 M urea in 50 mM ABC and then with pure water. Biotinylated peptides were eluted with 100 µl of 80% acetonitrile, 0.2% trifluoroacetic acid and 0.1% formic acid at 60°C five times. The combined elution fractions were dried using a Speed Vac and used for mass spectrometry analysis.

LC-MS/MS analysis of enriched peptide samples

Analytical capillary columns (100 cm×75 µm i.d.) and trap columns (2 cm×150 µm i.d.) were packed in-house with 3 µm Jupiter C18 particles (Phenomenex). The long analytical column was isothermally maintained at 45°C with a column heater (Analytical Sales and Services). A NanoAcquity UPLC system (Waters) was operated at a flow rate of 300 nl/min over 2 h with a linear gradient ranging from 95% solvent A (H_2O with 0.1% formic acid) to 40% solvent B (acetonitrile with 0.1% formic acid) for 100 min. The enriched peptide samples were analyzed using an Orbitrap Eclipse mass spectrometer (Thermo Fisher Scientific) equipped with an in-house customized nanoelectrospray ion source. Precursor ions were acquired (m/z 300–1500) at a 120 K resolving power and the isolation of the precursor for MS/MS analysis was performed with a 1.4 Th. High-energy collisional dissociation (HCD) with 30% collision energy was used for sequencing with an automatic gain control (AGC) target of 1e5. The resolving power for the acquired MS2 spectra was set to 30 K with dynamic maximum injection time.

MS data analysis

All MS/MS data were searched using MaxQuant (version 1.6.2.3) with the Andromeda search engine at a 10 ppm precursor ion mass tolerance against the Uniprot *Drosophila melanogaster* proteome database (42,824 entries; http://www.uniprot.org/). Label-free quantification (LFQ) and matching between runs were performed with the following search parameters: trypic digestion, fixed carbaminomethylation on cysteine, dynamic oxidation of methionine, dynamic protein N-terminal acetylation and dynamic biotin labels of lysine residues. A false discovery rate (FDR) of less than 1% was obtained for uniquely labeled peptides and proteins.

Bioinformatics

For data processing and visualization of mass spectrometry data, LFQ intensity values from MaxQuant were analyzed using the R package DEP which provides tools for filtering, variance normalization, imputation of missing values and statistical testing for differentially expressed proteins. For the analysis, we first filtered out proteins that contained missing values in any replicate for each condition. Background correction and normalization were performed using a variance-stabilizing transformation (vsn). Condition-specific missing values were imputed using a small deterministic value (R package Msnbase:MinDET method). The missing values were replaced with a minimal value observed in that sample, which is estimated as being the q-th quantile (default 'q=0.01' was used). Differential enrichment analysis (DEA) was performed by applying protein-wise linear models combined with empirical Bayes statistics between conditions (R package limma). The q-value was generated from raw *P*-values using R package qvalue for further differential enrichment analysis.

PPIs were derived from the Search Tool for the Retrieval of Interacting Genes/Proteins (STRING, stringApp v1.7 in Cytoscape v3.9.0-BETA1) database (confidence score cut-off value, 0.4; maximum additional interactors, 0). Clustering of the PPI networks was achieved using the Markov cluster algorithm (MCL; granular parameter, 4).

GO biological process and cellular component enrichment analyses were conducted using the ClueGO software (ClueGO v2.5.8 in Cytoscape v3.9.0-BETA1). Overview of total proteins with the data-centered per protein was visualized using a heatmap.

Acknowledgements

We are grateful to Dr Hyun-Woo Rhee for the APEX2 and TurboID plasmids and technical advice. We thank the laboratory members for discussions and help. Imaging was performed using the Zeiss LSM 710 confocal microscope available at the Soonchunhyang Biomedical Science Core-facility of Korea Basic Science Institute (KBSI).

Competing interests

The authors declare no competing or financial interests.

Author contributions

Conceptualization: T.T.M.N., J.-S.K., M.L.; Methodology: T.T.M.N., C.M., M.L.; Software: C.M., S.S., J.-S.K.; Validation: T.T.M.N., M.V.; Formal analysis: T.T.M.N., C.M., Jeesoo Kim, Y.K., S.S., J.-S.K., M.L.; Investigation: T.T.M.N., C.M., Jeesoo Kim, Y.K., M.V., S.J., H.-A.P.-B., Junhyung Kim, J.-S.K., M.L.; Resources: T.T.M.N., J.-S.K., M.L.; Data curation: C.M., Jeesoo Kim, Y.K., J.-S.K.; Writing - original draft: T.T.M.N., C.M., J.-S.K., M.L.; Writing - review & editing: J.-S.K., M.L.; Visualization: T.T.M.N., C.M., M.L.; Supervision: J.-S.K., M.L.; Project administration: J.-S.K., M.L.; Funding acquisition: J.-S.K., M.L.

Funding

This work was supported by National Research Foundation of Korea (NRF-2018R1C1B6006466 to M.L.; 2021R1A2C4002421 to M.L.; NRF-2022M3A9I2082294 to J.-S.K.; 2019M3E5D3073092 to M.L. and J.-S.K.), Institute for Basic Science from the Ministry of Science and ICT, South Korea (IBS-R008-D1 to J.-S.K.), Creative-Pioneering Researchers Program through Seoul National University (to J.-S.K.) and POSCO TJ Park Foundation (POSCO Science Fellowship to M.L.).

Data availability

The mass spectrometry proteomics data have been deposited to the ProteomeXchange Consortium via the PRIDE [1] partner repository with the dataset identifier PXD036182.

Peer review history

The peer review history is available online at https://journals.biologists.com/dev/lookup/doi/10.1242/dev.201220.reviewer-comments.pdf

References

Aravin, A. A., Hannon, G. J. and Brennecke, J. (2007). The Piwi-piRNA pathway provides an adaptive defense in the transposon arms race. *Science* **318**, 761-764. doi:10.1126/science.1146484

Baker, F. C., Neiswender, H., Veeranan-Karmegam, R. and Gonsalvez, G. B. (2021). In vivo proximity biotin ligation identifies the interactome of Egalitarian, a Dynein cargo adaptor. *Development* **148**, dev199935. doi:10.1242/dev.199935

Branon, T. C., Bosch, J. A., Sanchez, A. D., Udeshi, N. D., Svinkina, T., Carr, S. A., Feldman, J. L., Perrimon, N. and Ting, A. Y. (2018). Efficient proximity labeling in living cells and organisms with TurboID. *Nat. Biotechnol.* **36**, 880-887. doi:10.1038/nbt.4201

Brennecke, J., Aravin, A. A., Stark, A., Dus, M., Kellis, M., Sachidanandam, R. and Hannon, G. J. (2007). Discrete small RNA-generating loci as master regulators of transposon activity in Drosophila. *Cell* **128**, 1089-1103. doi:10.1016/j.cell.2007.01.043

Cappucci, U., Noro, F., Casale, A. M., Fanti, L., Berloco, M., Alagia, A. A., Grassi, L., Le Pera, L., Piacentini, L. and Pimpinelli, S. (2019). The Hsp70 chaperone is a major player in stress-induced transposable element activation. *Proc. Natl. Acad. Sci. USA* **116**, 17943-17950. doi:10.1073/pnas.1903936116

Cazzolli, R., Shemon, A. N., Fang, M. Q. and Hughes, W. E. (2006). Phospholipid signalling through phospholipase D and phosphatidic acid. *IUBMB Life* **58**, 457-461. doi:10.1080/15216540600871142

Chen, C.-L., Hu, Y., Udeshi, N. D., Lau, T. Y., Wirtz-Peitz, F., He, L., Ting, A. Y., Carr, S. A. and Perrimon, N. (2015). Proteomic mapping in live Drosophila tissues using an engineered ascorbate peroxidase. *Proc. Natl. Acad. Sci. USA* **112**, 12093-12098. doi:10.1073/pnas.1515623112

Choi, S.-Y., Huang, P., Jenkins, G. M., Chan, D. C., Schiller, J. and Frohman, M. A. (2006). A common lipid links Mfn-mediated mitochondrial fusion and SNARE-regulated exocytosis. *Nat. Cell Biol.* **8**, 1255-1262. doi:10.1038/ncb1487

Choi-Rhee, E., Schulman, H. and Cronan, J. E. (2004). Promiscuous protein biotinylation by Escherichia coli biotin protein ligase. *Protein Sci.* **13**, 3043-3050. doi:10.1110/ps.04911804

Czech, B. and Hannon, G. J. (2016). One loop to rule them all: the ping-pong cycle and piRNA-guided silencing. *Trends Biochem. Sci.* **41**, 324-337. doi:10.1016/j.tibs.2015.12.008

Czech, B., Preall, J. B., McGinn, J. and Hannon, G. J. (2013). A transcriptome-wide RNAi screen in the Drosophila ovary reveals factors of the germline piRNA pathway. *Mol. Cell* **50**, 749-761. doi:10.1016/j.molcel.2013.04.007

Czech, B., Munafò, M., Ciabrelli, F., Eastwood, E. L., Fabry, M. H., Kneuss, E. and Hannon, G. J. (2018). piRNA-guided genome defense: from biogenesis to silencing. *Annu. Rev. Genet.* **52**, 131-157. doi:10.1146/annurev-genet-120417-031441

Ding, D. and Chen, C. (2020). Zucchini: the key ingredient to unveil piRNA precursor processing†. *Biol. Reprod.* **103**, 452-454. doi:10.1093/biolre/ioaa090

Feltzin, V. L., Khaladkar, M., Abe, M., Parisi, M., Hendriks, G. J., Kim, J. and Bonini, N. M. (2015). The exonuclease Nibbler regulates age-associated traits and modulates piRNA length in Drosophila. *Aging Cell* **14**, 443-452. doi:10.1111/acel.12323

Fernández-Ulibarri, I., Vilella, M., Lázaro-Diéguez, F., Sarri, E., Martínez, S. E., Jiménez, N., Claro, E., Mérida, I., Burger, K. N. J. and Egea, G. (2007). Diacylglycerol is required for the formation of COPI vesicles in the Golgi-to-ER transport pathway. *Mol. Biol. Cell* **18**, 3250-3263. doi:10.1091/mbc.e07-04-0334

Ge, D. T., Wang, W., Tipping, C., Gainetdinov, I., Weng, Z. and Zamore, P. D. (2019). The RNA-binding ATPase, armitage, couples piRNA amplification in nuage to phased piRNA production on mitochondria. *Mol. Cell* **74**, 982-995.e986. doi:10.1016/j.molcel.2019.04.006

Gunawardane, L. S., Saito, K., Nishida, K. M., Miyoshi, K., Kawamura, Y., Nagami, T., Siomi, H. and Siomi, M. C. (2007). A slicer-mediated mechanism for repeat-associated siRNA 5′ end formation in Drosophila. *Science* **315**, 1587-1590. doi:10.1126/science.1140494

Haase, A. D., Fenoglio, S., Muerdter, F., Guzzardo, P. M., Czech, B., Pappin, D. J., Chen, C., Gordon, A. and Hannon, G. J. (2010). Probing the initiation and effector phases of the somatic piRNA pathway in Drosophila. *Genes Dev.* **24**, 2499-2504. doi:10.1101/gad.1968110

Han, S., Li, J. and Ting, A. Y. (2018). Proximity labeling: spatially resolved proteomic mapping for neurobiology. *Curr. Opin. Neurobiol.* **50**, 17-23. doi:10.1016/j.conb.2017.10.015

Handler, D., Meixner, K., Pizka, M., Lauss, K., Schmied, C., Gruber, F. S. and Brennecke, J. (2013). The genetic makeup of the Drosophila piRNA pathway. *Mol. Cell* **50**, 762-777. doi:10.1016/j.molcel.2013.04.031

Hayashi, R., Schnabl, J., Handler, D., Mohn, F., Ameres, S. L. and Brennecke, J. (2016). Genetic and mechanistic diversity of piRNA 3′-end formation. *Nature* **539**, 588-592. doi:10.1038/nature20162

Hensen, F., Moretton, A., van Esveld, S., Farge, G. and Spelbrink, J. N. (2018). The mitochondrial outer-membrane location of the EXD2 exonuclease contradicts its direct role in nuclear DNA repair. *Sci. Rep.* **8**, 5368. doi:10.1038/s41598-018-23690-y

Höck, J. and Meister, G. (2008). The Argonaute protein family. *Genome Biol.* **9**, 210. doi:10.1186/gb-2008-9-2-210

Huang, H., Gao, Q., Peng, X., Choi, S.-Y., Sarma, K., Ren, H., Morris, A. J. and Frohman, M. A. (2011). piRNA-associated germline nuage formation and spermatogenesis require MitoPLD profusogenic mitochondrial-surface lipid signaling. *Dev. Cell* **20**, 376-387. doi:10.1016/j.devcel.2011.01.004

Huang, X., Fejes Tóth, K. and Aravin, A. A. (2017). piRNA Biogenesis in Drosophila melanogaster. *Trends Genet.* **33**, 882-894. doi:10.1016/j.tig.2017.09.002

Hung, V., Lam, S. S., Udeshi, N. D., Svinkina, T., Guzman, G., Mootha, V. K., Carr, S. A. and Ting, A. Y. (2017). Proteomic mapping of cytosol-facing outer mitochondrial and ER membranes in living human cells by proximity biotinylation. *eLife* **6**, e24463. doi:10.7554/eLife.24463

Hutvagner, G. and Simard, M. J. (2008). Argonaute proteins: key players in RNA silencing. *Nat. Rev. Mol. Cell Biol.* **9**, 22-32. doi:10.1038/nrm2321

Ipsaro, J. J., Haase, A. D., Knott, S. R., Joshua-Tor, L. and Hannon, G. J. (2012). The structural biochemistry of Zucchini implicates it as a nuclease in piRNA biogenesis. *Nature* **491**, 279-283. doi:10.1038/nature11502

Iwasaki, Y. W., Siomi, M. C. and Siomi, H. (2015). PIWI-interacting RNA: its biogenesis and functions. *Annu. Rev. Biochem.* **84**, 405-433. doi:10.1146/annurev-biochem-060614-034258

Izumi, N., Kawaoka, S., Yasuhara, S., Suzuki, Y., Sugano, S., Katsuma, S. and Tomari, Y. (2013). Hsp90 facilitates accurate loading of precursor piRNAs into PIWI proteins. *RNA* **19**, 896-901. doi:10.1261/rna.037200.112

Karam, J. A., Parikh, R. Y., Nayak, D., Rosenkranz, D. and Gangaraju, V. K. (2017). Co-chaperone Hsp70/Hsp90-organizing protein (Hop) is required for transposon silencing and Piwi-interacting RNA (piRNA) biogenesis. *J. Biol. Chem.* **292**, 6039-6046. doi:10.1074/jbc.C117.777730

Le Thomas, A., Tóth, K. F. and Aravin, A. A. (2014). To be or not to be a piRNA: genomic origin and processing of piRNAs. *Genome Biol.* **15**, 204. doi:10.1186/gb4154

Lee, S.-Y., Kang, M.-G., Shin, S., Kwak, C., Kwon, T., Seo, J. K., Kim, J.-S. and Rhee, H.-W. (2017). Architecture mapping of the inner mitochondrial membrane proteome by chemical tools in live cells. *J. Am. Chem. Soc.* **139**, 3651-3662. doi:10.1021/jacs.6b10418

Lim, A. K. and Kai, T. (2007). Unique germ-line organelle, nuage, functions to repress selfish genetic elements in Drosophila melanogaster. *Proc. Natl. Acad. Sci. USA* **104**, 6714-6719. doi:10.1073/pnas.0701920104

Liu, Y., Dou, M., Song, X., Dong, Y., Liu, S., Liu, H., Tao, J., Li, W., Yin, X. and Xu, W. (2019). The emerging role of the piRNA/piwi complex in cancer. *Mol. Cancer* **18**, 123. doi:10.1186/s12943-019-1052-9

Ma, L., Buchold, G. M., Greenbaum, M. P., Roy, A., Burns, K. H., Zhu, H., Han, D. Y., Harris, R. A., Coarfa, C., Gunaratne, P. H. et al. (2009). GASZ is essential for male meiosis and suppression of retrotransposon expression in the male germline. *PLoS Genet.* **5**, e1000635. doi:10.1371/journal.pgen.1000635

Malone, C. D., Brennecke, J., Dus, M., Stark, A., McCombie, W. R., Sachidanandam, R. and Hannon, G. J. (2009). Specialized piRNA pathways act in germline and somatic tissues of the Drosophila ovary. *Cell* **137**, 522-535. doi:10.1016/j.cell.2009.03.040

Mannix, K. M., Starble, R. M., Kaufman, R. S. and Cooley, L. (2019). Proximity labeling reveals novel interactomes in live Drosophila tissue. *Development* **146**, dev176644. doi:10.1242/dev.176644

Mehla, J., Caufield, J. H., Sakhawalkar, N. and Uetz, P. (2017). A comparison of two-hybrid approaches for detecting protein-protein interactions. *Methods Enzymol.* **586**, 333-358. doi:10.1016/bs.mie.2016.10.020

Munafò, M., Manelli, V., Falconio, F. A., Sawle, A., Kneuss, E., Eastwood, E. L., Seah, J. W. E., Czech, B. and Hannon, G. J. (2019). Daedalus and Gasz recruit Armitage to mitochondria, bringing piRNA precursors to the biogenesis machinery. *Genes Dev.* **33**, 844-856. doi:10.1101/gad.325662.119

Nguyen, T. M. T., Kim, J., Doan, T. T., Lee, M.-W. and Lee, M. (2020). APEX proximity labeling as a versatile tool for biological research. *Biochemistry* **59**, 260-269. doi:10.1021/acs.biochem.9b00791

Nishimasu, H., Ishizu, H., Saito, K., Fukuhara, S., Kamatani, M. K., Bonnefond, L., Matsumoto, N., Nishizawa, T., Nakanaga, K., Aoki, J. et al. (2012). Structure and function of Zucchini endoribonuclease in piRNA biogenesis. *Nature* **491**, 284-287. doi:10.1038/nature11509

Olivieri, D., Senti, K.-A., Subramanian, S., Sachidanandam, R. and Brennecke, J. (2012). The cochaperone shutdown defines a group of biogenesis factors essential for all piRNA populations in Drosophila. *Mol. Cell* **47**, 954-969. doi:10.1016/j.molcel.2012.07.021

Ozata, D. M., Gainetdinov, I., Zoch, A., O'Carroll, D. and Zamore, P. D. (2019). PIWI-interacting RNAs: small RNAs with big functions. *Nat. Rev. Genet.* **20**, 89-108. doi:10.1038/s41576-018-0073-3

Pandey, R. R., Homolka, D., Chen, K.-M., Sachidanandam, R., Fauvarque, M.-O. and Pillai, R. S. (2017). Recruitment of Armitage and Yb to a transcript triggers its phased processing into primary piRNAs in Drosophila ovaries. *PLoS Genet.* **13**, e1006956. doi:10.1371/journal.pgen.1006956

Pane, A., Wehr, K. and Schüpbach, T. (2007). zucchini and squash encode two putative nucleases required for rasiRNA production in the Drosophila germline. *Dev. Cell* **12**, 851-862. doi:10.1016/j.devcel.2007.03.022

Park, J., Lee, S.-Y., Jeong, H., Kang, M.-G., Van Haute, L., Minczuk, M., Seo, J. K., Jun, Y., Myung, K., Rhee, H.-W. et al. (2019). The structure of human EXD2 reveals a chimeric 3′ to 5′ exonuclease domain that discriminates substrates via metal coordination. *Nucleic Acids Res.* **47**, 7078-7093. doi:10.1093/nar/gkz454

Preall, J. B., Czech, B., Guzzardo, P. M., Muerdter, F. and Hannon, G. J. (2012). shutdown is a component of the Drosophila piRNA biogenesis machinery. *RNA* **18**, 1446-1457. doi:10.1261/rna.034405.112

Qi, H., Watanabe, T., Ku, H.-Y., Liu, N., Zhong, M. and Lin, H. (2011). The Yb body, a major site for Piwi-associated RNA biogenesis and a gateway for Piwi expression and transport to the nucleus in somatic cells. *J. Biol. Chem.* **286**, 3789-3797. doi:10.1074/jbc.M110.193888

Qin, W., Cho, K. F., Cavanagh, P. E. and Ting, A. Y. (2021). Deciphering molecular interactions by proximity labeling. *Nat. Methods* **18**, 133-143. doi:10.1038/s41592-020-01010-5

Rhee, H.-W., Zou, P., Udeshi, N. D., Martell, J. D., Mootha, V. K., Carr, S. A. and Ting, A. Y. (2013). Proteomic mapping of mitochondria in living cells via spatially restricted enzymatic tagging. *Science* **339**, 1328-1331. doi:10.1126/science.1230593

Rogers, A. K., Situ, K., Perkins, E. M. and Toth, K. F. (2017). Zucchini-dependent piRNA processing is triggered by recruitment to the cytoplasmic processing machinery. *Genes Dev.* **31**, 1858-1869. doi:10.1101/gad.303214.117

Roux, K. J., Kim, D. I., Raida, M. and Burke, B. (2012). A promiscuous biotin ligase fusion protein identifies proximal and interacting proteins in mammalian cells. *J. Cell Biol.* **196**, 801-810. doi:10.1083/jcb.201112098

Saito, K., Ishizu, H., Komai, M., Kotani, H., Kawamura, Y., Nishida, K. M., Siomi, H. and Siomi, M. C. (2010). Roles for the Yb body components Armitage and Yb in primary piRNA biogenesis in Drosophila. *Genes Dev.* **24**, 2493-2498. doi:10.1101/gad.1989510

Shpiz, S., Ryazansky, S., Olovnikov, I., Abramov, Y. and Kalmykova, A. (2014). Euchromatic transposon insertions trigger production of novel Pi- and endo-siRNAs at the target sites in the drosophila germline. *PLoS Genet.* **10**, e1004138. doi:10.1371/journal.pgen.1004138

Sokolova, O. A., Yakushev, E. Y., Stolyarenko, A. D., Mikhaleva, E. A., Gvozdev, V. A. and Klenov, M. S. (2011). Interplay of transposon-silencing genes in the germline of Drosophila melanogaster. *Mol. Biol.* **45**, 582-590. doi:10.1134/S0026893311030174

Specchia, V., Piacentini, L., Tritto, P., Fanti, L., D'Alessandro, R., Palumbo, G., Pimpinelli, S. and Bozzetti, M. P. (2010). Hsp90 prevents phenotypic variation by suppressing the mutagenic activity of transposons. *Nature* **463**, 662-665. doi:10.1038/nature08739

Starr, M. L., Sparks, R. P., Arango, A. S., Hurst, L. R., Zhao, Z., Lihan, M., Jenkins, J. L., Tajkhorshid, E. and Fratti, R. A. (2019). Phosphatidic acid induces conformational changes in Sec18 protomers that prevent SNARE priming. *J. Biol. Chem.* **294**, 3100-3116. doi:10.1074/jbc.RA118.006552

Story, B., Ma, X., Ishihara, K., Li, H., Hall, K., Peak, A., Anoja, P., Park, J., Haug, J., Blanchette, M. et al. (2019). Defining the expression of piRNA and transposable elements in Drosophila ovarian germline stem cells and somatic support cells. *Life Sci. Alliance* **2**, e201800211. doi:10.26508/lsa.201800211

ten Have, S., Boulon, S., Ahmad, Y. and Lamond, A. I. (2011). Mass spectrometry-based immuno-precipitation proteomics - the user's guide. *Proteomics* **11**, 1153-1159. doi:10.1002/pmic.201000548

Uçkun, E., Wolfstetter, G., Anthonydhason, V., Sukumar, S. K., Umapathy, G., Molander, L., Fuchs, J. and Palmer, R. H. (2021). In vivo profiling of the Alk proximitome in the developing Drosophila brain. *J. Mol. Biol.* **433**, 167282. doi:10.1016/j.jmb.2021.167282

Vagin, V. V., Yu, Y., Jankowska, A., Luo, Y., Wasik, K. A., Malone, C. D., Harrison, E., Rosebrock, A., Wakimoto, B. T., Fagegaltier, D. et al. (2013). Minotaur is critical for primary piRNA biogenesis. *RNA* **19**, 1064-1077. doi:10.1261/rna.039669.113

Varnaitė, R. and MacNeill, S. A. (2016). Meet the neighbors: mapping local protein interactomes by proximity-dependent labeling with BioID. *Proteomics* **16**, 2503-2518. doi:10.1002/pmic.201600123

Vicogne, J., Vollenweider, D., Smith, J. R., Huang, P., Frohman, M. A. and Pessin, J. E. (2006). Asymmetric phospholipid distribution drives in vitro reconstituted SNARE-dependent membrane fusion. *Proc. Natl. Acad. Sci. USA* **103**, 14761-14766. doi:10.1073/pnas.0606881103

Voronina, E., Seydoux, G., Sassone-Corsi, P. and Nagamori, I. (2011). RNA granules in germ cells. *Cold Spring Harb. Perspect. Biol.* **3**, a002774. doi:10.1101/cshperspect.a002774

Wang, C. and Lin, H. (2021). Roles of piRNAs in transposon and pseudogene regulation of germline mRNAs and lncRNAs. *Genome Biol.* **22**, 27. doi:10.1186/s13059-020-02221-x

Watanabe, T. and Lin, H. (2014). Posttranscriptional regulation of gene expression by Piwi proteins and piRNAs. *Mol. Cell* **56**, 18-27. doi:10.1016/j.molcel.2014.09.012

Watanabe, T., Chuma, S., Yamamoto, Y., Kuramochi-Miyagawa, S., Totoki, Y., Toyoda, A., Hoki, Y., Fujiyama, A., Shibata, T., Sado, T. et al. (2011). MITOPLD is a mitochondrial protein essential for nuage formation and piRNA biogenesis in the mouse germline. *Dev. Cell* **20**, 364-375. doi:10.1016/j.devcel.2011.01.005

Xiol, J., Cora, E., Koglgruber, R., Chuma, S., Subramanian, S., Hosokawa, M., Reuter, M., Yang, Z., Berninger, P., Palencia, A. et al. (2012). A role for Fkbp6 and the chaperone machinery in piRNA amplification and transposon silencing. *Mol. Cell* **47**, 970-979. doi:10.1016/j.molcel.2012.07.019

Yamashiro, H., Negishi, M., Kinoshita, T., Ishizu, H., Ohtani, H. and Siomi, M. C. (2020). Armitage determines Piwi-piRISC processing from precursor formation and quality control to inter-organelle translocation. *EMBO Rep.* **21**, e48769. doi:10.15252/embr.201948769

Yang, J.-S., Gad, H., Lee, S. Y., Mironov, A., Zhang, L., Beznoussenko, G. V., Valente, C., Turacchio, G., Bonsra, A. N., Du, G. et al. (2008). A role for phosphatidic acid in COPI vesicle fission yields insights into Golgi maintenance. *Nat. Cell Biol.* **10**, 1146-1153. doi:10.1038/ncb1774

Zhang, B., Zhang, Y. and Liu, J.-L. (2021). Highly effective proximate labeling in Drosophila. *G3 (Bethesda)* **11**, jkab077. doi:10.1093/g3journal/jkab077

Zhang, Z., Xu, J., Koppetsch, B. S., Wang, J., Tipping, C., Ma, S., Weng, Z., Theurkauf, W. E. and Zamore, P. D. (2011). Heterotypic piRNA Ping-Pong requires qin, a protein with both E3 ligase and Tudor domains. *Mol. Cell* **44**, 572-584. doi:10.1016/j.molcel.2011.10.011

Zhang, Y., Liu, X., Bai, J., Tian, X., Zhao, X., Liu, W., Duan, X., Shang, W., Fan, H.-Y. and Tong, C. (2016). Mitoguardin regulates mitochondrial fusion through MitoPLD and is required for neuronal homeostasis. *Mol. Cell* **61**, 111-124. doi:10.1016/j.molcel.2015.11.017

Zhukovsky, M. A., Filograna, A., Luini, A., Corda, D. and Valente, C. (2019). Phosphatidic acid in membrane rearrangements. *FEBS Lett.* **593**, 2428-2451. doi:10.1002/1873-3468.13563